CONTRIBUTED PAPER

Solution-Processed Quantum Dot Photodetectors

Flexible thin-film photodetectors for imaging systems, including those suitable for video applications, can handle visible light and also enter the infrared spectral region.

By Gerasimos Konstantatos and Edward H. Sargent

ABSTRACT | Digital imaging has traditionally been enabled by single-crystalline photodetectors. This approach typically either mandates the use of silicon as photon-to-electron converter or requires a hybrid-integrated solution. In contrast, solution-processed optoelectronic materials offer convenient integration of light-sensing materials atop an electronic readout circuit. Colloidal quantum dots offer particular advantages, combining solution-processing with the spectral tunability afforded by the quantum size effect. Here we review recent progress in solution-processed quantum dot photodetectors and their application in future imaging systems. We focus on progress towards high responsivity (photon-to-electron gains exceeding 1000) and sensitivity (normalized detectivity $D^* \sim 10^{13}$ Jones) in the visible, the near infrared, and the short-wavelength infrared. We also highlight the achievement of solution-processed photoconductive photodetectors combining photoconductive gain and temporal responses faster than 30 ms, devices therefore compatible with video-frame-rate imaging. We conclude with a discussion of recent colloidal quantum dot photodiodes having megahertz bandwidth and detectivity of 10^{11} Jones.

KEYWORDS | Nanocrystals; photodetectors; quantum dots; solution-processed

I. INTRODUCTION

A. Applications of Top-Surface Photodetectors

Optical communications, remote sensing, spectroscopy, and imaging are just few of the applications enabled by the detection of optical signals. Here we focus on imaging, a huge commercial sector, and ubiquitous consumer product.

The advent of digital imaging and media has rendered photography and video capture widespread. A photosensitive material is required to absorb optical signals in the visible range (i.e., wavelengths of 400–700 nm) and transform them into electronic signals. Visible imaging applications also include surveillance, machine vision, industrial inspection, spectroscopy, and fluorescent biomedical imaging.

Sensitive photodetection in the short wavelength infrared (SWIR), on the other hand, enables passive night vision [1], [2] from 1 to 1.7 μm and biomedical imaging for tumor detection [3] exploiting the tissue transparent windows around 900 and 1100 nm [4], [5]. Additional applications of SWIR imaging can be found in astrophysics [6], in remote sensing for climate and natural resources monitoring [7], and in food and pharmaceutical industries for quality control and product inspection [8] and identification [9].

The combination of visible and infrared detection towards multispectral imaging provides a powerful tool that offers independent pieces of information extracted from the interaction of light of different wavelengths with matter. Such functionality is of limited use today due to the high fabrication cost and modest performance of such photodetectors. Present-day multispectral image sensors are required to embed on a single platform various semiconductor processes that are not monolithically integrable. This results in high complexity, high cost, and a sacrifice in performance [10].

B. Requirements for High-Quality Video Imaging

At this point we briefly discuss the fundamental specifications a photodetector should satisfy to be considered a candidate for imaging applications.

The first feature of a photodetector is sensitivity, the capacity of a detector to distinguish an incident optical

Manuscript received October 21, 2008. Current version published September 16, 2009.
G. Konstantatos is with the Department of Electrical and Computer Engineering, University of Toronto, Toronto, ON M5S 3G4, Canada. He is also with Institut de Ciencies Fotoniques, Parc Mediterrani de la Tecnologia, 08860 Barcelona, Spain (e-mail: ger.konstantatos@utoronto.ca).
E. H. Sargent is with the Department of Electrical and Computer Engineering, University of Toronto, Toronto, ON M5S 3G4, Canada (e-mail: ted.sargent@utoronto.ca).
Digital Object Identifier: 10.1109/JPROC.2009.2025612

signal from noise. In the section that follows, we present several quantitative figures of merit that allow comparison amongst different detector technologies. Higher sensitivity enables imaging at lower levels of illumination and higher image signal-to-noise under brighter illumination.

True-to-life video capture requires sampling images at a frame rate that matches the eye's refresh rate. To avoid the appearance of ghosting, the temporal response of the photodetector must be sufficiently rapid that, within a period of a small number of frames (typically five), no photocurrent remnant remains that is perceptible by the human eye. The photocurrent time constant of the detector should, thus, be no longer than a few tens of milliseconds. Still-imaging applications can tolerate longer temporal responses if a shutter is employed and if the benefit in sensitivity compensates for the loss of temporal fidelity.

When it comes to practical implementation of an image sensor technology, the issue of convenient integration of sensing materials with readout electronics comes to the forefront. Ideally, a photosensitive material should be readily monolithically integrated with a simple, low-cost CMOS readout integrated circuit, offering low fabrication cost, low complexity, and high pixel count.

Imaging in the visible is largely facilitated by silicon photodiodes. Early imaging arrays were based on charge-coupled devices (CCDs). This approach involves a photoactive sensor array with several stages of photocharge transfer to the readout circuit for electronic processing. For this purpose, the interconnection of two chips is required to transfer the photocharge from the sensor to the electronic circuitry. CCD cameras offer a fill factor—the ratio of the optically active area of the chip to its total area—that may vary from 100% to 50% depending on the cell design [11]. CCDs are prone to high fabrication and integration cost due to multiple chip interconnections and the incompatibility of CMOS with the process required for the CCD platform.

In 1997, an integrated CMOS image sensor was reported on a single chip for optical sensing and signal processing [12]. Its fill factor was limited to 30% due to the coexistence of photoactive elements and readout circuitry on the same chip. Amorphous silicon photodetectors have been proposed as a top-surface photodetector with promise for 100% fill factor [13]. However, these suffer from long time constants [14] and material instabilities under illumination [15].

Silicon photodiodes demonstrate superb transient time in the nanoseconds, well exceeding the requirements for imaging applications. Their photodiode mechanism of operation limits their internal quantum efficiency to 100% since at most one charge carrier is extracted for each absorbed photon. Their sensitivity is thus susceptible to the readout circuit noise. In order to overcome this limit, Si avalanche photodiodes have been proposed for use in CMOS image sensors [16]. The high required applied bias, however, curtails their integration in conventional CMOS circuits. Further design considerations are required to suppress the high leakage currents present in such structures [17].

For sensing and imaging in the SWIR, the use of InGaAs photodiodes leads the market. $In_{0.53}Ga_{0.47}As$ lattice matched with InP and with bandgap of 0.73 eV addresses the SWIR spectrum and is suited for night vision applications. Their sensitivity is very high, with noise equivalent intensity (minimum light intensity that can be detected) on the order of a few pW/cm^2, and their transient response provides frame rates up to several kframes/second. The molecular beam epitaxy technique required for the growth of InGaAs imposes a high materials cost per unit area of sensor. Hybrid integration of the light-sensing InGaAs array requires bump-bonding techniques that increase the cost further and also limit the pixel resolution to a few hundreds of kpixels. The typical price for a night vision camera based on InGaAs is ~$40 000. Moreover, conventional InGaAs-on-InP-substrate sensitivity drops dramatically at wavelengths shorter than 900 nm due to substrate absorption, making it impractical for visible imaging applications.

The advent of self-assembled epitaxially grown quantum dots has also led to dramatic progress in the development of quantum dot infrared photodetectors. This technology has been employed to address the challenges of mid- and long-wavelength infrared detectors for sensing and imaging [18], [19]. Quantum dots show promise for narrow spectral response reduced dark current and thereby higher detectivities with higher temperature operation compared to the quantum-well counterparts [20], [21].

The development of a CMOS-compatible infrared detector has been undertaken by growing germanium on silicon. Even though these devices require costly epitaxial growth techniques, they show promise for monolithic integration of infrared detectors on CMOS. SiGe photodiodes have been reported with infrared sensitivity [22]. These detectors were developed with emphasis on high-speed performance for optical communications and exhibit bandwidths in excess of 1 GHz [23]; their responsivity, however, was reported ~0.1 A/W, resulting in insufficient sensitivity for imaging applications (D^* is found ~10^8 Jones). Their integration onto CMOS focal plane arrays for imaging was also reported [24]. SiGe technology, promising as it is, requires further efforts towards successful fabrication of sensitive imaging systems.

C. Colloidal Quantum Dots for Light Detection

Colloidal quantum dots have recently attracted significant attention as a candidate material for a range of optoelectronic applications. Light-emitting diodes [25], [26], lasers [27], optical modulators [28], solar cells [29], [30], and photodetectors [31] have all been reported. One major benefit of colloidal quantum dots arises from their solution processibility: this facilitates ready integration with an almost limitless variety of substrates, including

postprocessing atop other integrated circuits. Additionally, quantum dots' optical absorption and emission spectra are widely tunable through the quantum size effect [32]. The impact of these traits on photodetector technology is discussed in this section.

Device fabrication based on conventional single-crystalline semiconductors such as silicon and InGaAs requires high-temperature processing and high-vacuum conditions accompanied by high-cost equipment. Monolithically integrated optoelectronics also mandates growth on crystalline substrates using lattice-matched semiconductors. Unlike electronic devices, low-cost optoelectronic devices are therefore hard to achieve in view of materials incompatibilities and highly customized deposition systems.

The realization of thin-film top-surface photodetectors offers the field of flexible electronics new functions to deliver atop its low cost, lightweight, flexible platform. Recent progress in organic transistors and their integration [33] has led to the demonstration of various large area, flexible, low cost, portable sensors [34], [35] and displays [36]. Conventional single-crystalline semiconductors are precluded from integration with flexible organic electronics due to the incompatibility of their growth conditions with the process windows required by organic semiconductors. Their upscaling from silicon-wafer-area to larger area applications is also limited by the serialized nature of wafer processing, in contrast with the roll-to-roll processing of sheets of flexible substrates.

Solution-synthesized colloidal quantum dots can readily be deposited using spin-coating, spray-casting, or inkjet printing techniques on any substrate conducting or insulating, crystalline or amorphous, rigid or flexible. Lattice mismatch considerations do not arise, and large-area processing is facilitated by roll-to-roll processing onto flexible substrates. Colloidal nanocrystals (NCs) are synthesized using wet chemistry techniques: reagents are injected into a flask and, through control of reagent concentrations, ligand selection, and temperature, nanocrystals of a desired size and shape can be delivered. Synthesis and growth of nanocrystals of the desired size is followed by isolation and redispersion in organic solvents for subsequent solution processing. As an example, Fig. 1 demonstrates the application of colloidal quantum dots in the fabrication of a monolithically integrated sensor array. Nanocrystals from solution are spin-coated on a readout integrated circuit (ROIC). Individual pixels are delineated by the area of the metal pads presented on the top surface of the ROIC. After nanocrystal film deposition, a transparent conductive oxide is deposited to form biased photodetectors. This architecture, called top-surface photodetector, is compatible with postprocessing atop CMOS electronics and offers a 100% fill factor since all the area of the chip can be used for light sensing.

The ability to control the spectrum of absorption or emission in optoelectronic devices is useful in many

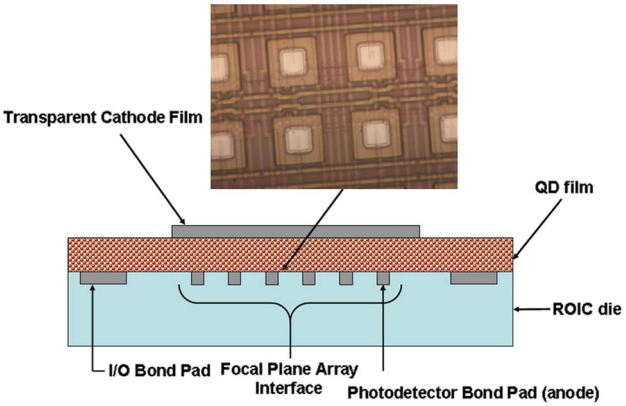

Fig. 1. ***Demonstration of a sensor array structure based on colloidal quantum dots.***

applications: lasers with tunable spectrum can be employed for wavelength-division multiplex optical communications systems [37]; light-emitting diodes that combine red, green, and blue light can be used for white light illumination for displays and high-efficiency lighting systems [38].

In photodetectors, spectral tunability eliminates the need for optical filters to address the spectrum of interest, leading to lower cost implementation and avoiding loss of signal that arises when filtering and sensing are implemented in series rather than within a single spectrally selective sensing medium. Furthermore, the absorption onset of the detector can be selected to match the longer wavelength of the intended spectrum. This avoids absorption of longer wavelength photons that are not of interest in certain imaging applications but that do contribute excess noise.

In bulk semiconductors, wavelength tunability is achieved via changes in the stoichiometry of ternary or quaternary compounds ($In_xGa_{1-x}As_yP_{1-y}$). This introduces extra complexity during growth. Colloidal quantum dots offer quantum size effect tuning wherein the absorption onset (as determined by the first excitonic peak) as well as the emission spectrum may be controlled through the size of the nanocrystals. It is possible, therefore, to achieve tunable emission and absorption from a single material quantum dot system to address various spectral windows.

Fig. 2 illustrates the tunability in absorption offered by PbS colloidal nanocrystals. By varying the dot size from ~10 to ~2 nm in diameter, the whole SWIR and visible spectrum can be selectively addressed from 1800 to 700 nm. PbS quantum dot photodetectors can address spectral windows of interest in a range of important applications: visible for video and photography; near-infrared for biomedical imaging; SWIR for night vision applications, and all of the above for spectroscopy and broadband applications. We exploit the wide-ranging

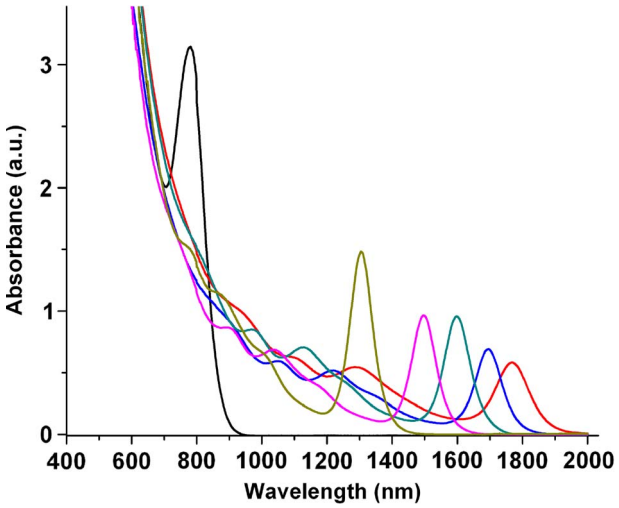

Fig. 2. *Quantum size effect tunability of the absorption spectrum in PbS colloidal quantum dots. The quantum dot size varies from 10 nm (red) to 3 nm (black) in diameter.*

tunability of PbS in this paper to demonstrate multispectral photodetection.

II. FUNDAMENTALS OF PHOTODETECTORS

A. Types of Photodetectors

There are two main classes of photodetectors: the photoconductors and the photodiodes.

A photoconductor typically consists of a semiconducting material, single-crystalline, polycrystalline or amorphous, and two ohmic metal contacts to form a two-port electrical device. Upon illumination, the conductivity of the material changes due to a change in mobility or carrier density or both [39]. Conductivity increase upon illumination is most typically attributed to generation of electron-hole pairs resulting in a carrier density increase. Photoconductors offer photoconductive gain, a greater-than-unity ratio of the number of circulated charge carriers per absorbed photon. The physical mechanism underlying photoconductive gain has been extensively studied [40], [41]. The trap states that contribute to photosensitization, also called sensitizing centers, favor the capture of one carrier (e.g., electrons) over the other (e.g., holes). Upon photoexcitation, electrons are captured by these centers, whereas holes remain free to traverse the device. The low capture probability for holes prolongs their carrier lifetime. The holes, upon reaching one contact, can be replenished by the other contact. The number of passes of a hole across the device is then equal to the ratio of the carrier lifetime to its transit time, giving rise to photoconductive gain G equal to τ_p/τ_{trp}. A thorough investigation of the implications of this mechanism on the optoelectronic characteristics of such detectors is discussed by Rose *et al.* [42]–[44].

Photodiodes, on the other hand, are based on the formation of a junction between two different semiconductors (heterojunctions), or a semiconductor with opposite doping levels (homojunction), or a semiconductor and a rectifying metal contact (Schottky junction). In each case, the principle is separation of photogenerated electron-hole pairs by the action of the built-in electric field in the junction and transport of the carriers to the respective contacts for extraction. This principle ensures that photodiodes are limited in their quantum efficiency to one carrier extracted per absorbed photon. At the same time, since photodiodes' temporal response is determined by the transit time of the carriers, and not their lifetime, photodiodes are often faster than photoconductors.

B. Figures of Merit

A set of figures of merit has been formulated to evaluate various photodetector technologies for sensing applications [45].

The concept of responsivity has been introduced to quantify the electrical signal output of the detector per optical signal input. Responsivity R is the ratio of photocurrent to the optical power impinging on the detector and measured thus in A/W. The general expression for responsivity is given by

$$R = \frac{\eta q \lambda}{hc} \frac{1}{\sqrt{1+\omega^2\tau^2}} G \tag{1}$$

where q is the electron charge, h is Planck's constant c is the speed of light, ω is the electrical modulation frequency, η is the quantum efficiency, τ is the time constant, and G is the photoconductive gain.

The quantum efficiency is defined as the efficiency with which an incident photon results in the excitation of an electron. It is a normalized value and is equal to the number of electrons excited divided by the number of photons incident on the detector's active area. Typically, quantum efficiency takes into account reflectance, absorbance, and scattering. In this case, it may be also called external quantum efficiency (EQE). In photoconductive photodetectors, the time constant that determines the 3-dB bandwidth of responsivity is related to the carrier lifetimes introduced by the associated sensitizing trap states.

Another important parameter in the characterization of photodetector in order to estimate its sensitivity is noise. There exist four major sources of noise in photoconductors: Johnson noise, shot noise, generation-recombination (G-R) noise, and $1/f$ noise [45].

By taking together the responsivity and the noise performance of the detector, one can quantify the ultimate figure of merit of sensitivity. The minimum optical power

level a detector can discern depends on the responsivity and the noise level. The signal current produced by the input power must be above the noise level in order to be detected. The signal-to-noise ratio (SNR) is given by

$$\mathrm{SNR} = \frac{RP}{i_n} \tag{2}$$

where R is responsivity, P is the incident optical power, and i_n is the noise current. The optical power at which the SNR is equal to unity is the minimum optical power that the detector can discern. It is called noise equivalent power (NEP) and is given by

$$\mathrm{NEP} = \frac{i_n}{R}. \tag{3}$$

The disadvantage of using NEP to describe detector performance is that it is specific to detectors having a particular surface area.

The figure of merit D^* called normalized or specific detectivity [46] is widely used as a descriptor of detector's sensitivity that is insensitive to device area. This parameter allows for comparison among detectors of different geometries, thus enabling the evaluation of sensitivity of photoconductive materials rather than specific devices. The expression for D^* is given by

$$D^* = \frac{\sqrt{A_d B}}{\mathrm{NEP}} = \frac{\sqrt{A_d B}R}{i_n} \tag{4}$$

where A_d is the detector's area, B is the electrical bandwidth, R is the responsivity, i_n is the noise current, and NEP is the noise equivalent power. The units of D^* are cm-$\mathrm{Hz}^{1/2}\mathrm{W}^{-1}$ or Jones. It can be interpreted as the SNR produced by a detector of 1 cm^2 surface when 1 W of opfctical power impinges, measured with electrical bandwidth of 1 Hz. Similarly to responsivity, D^* is also a function of many parameters: applied bias, temperature, modulation frequency, and wavelength; D^* should also then be reported followed by the measurement conditions.

III. PRIOR ART IN SOLUTION-PROCESSED PHOTODETECTORS

The attractive features of solution processibility have been exploited towards large area, low cost, flexible thin-film optoelectronic devices. Photodetectors have thus been reported from conjugated polymers and colloidal nanocrystals. We now present a review of the literature to demonstrate the progress in the field and also to establish the challenges to be addressed.

In 1994, Heeger *et al.* reported the realization of solution-processed photodetectors based on conjugated polymers [47]. The photodiodes consisted of P3OT or MEH-PPV—C60 (fullerenes) composite, spin-coated on an indium tin oxide (ITO) covered glass substrate followed by metal evaporation of the cathode. The devices were sensitive to visible and ultraviolet and demonstrated responsivity of 0.3 A/W across this spectral range. C60 was employed to facilitate extension of sensitivity to 700 nm, but no longer than this. The required applied bias of the device was 10 V. A large-area full-color image sensor based on polymer composites was reported four years later [48]. The active layer consisted of a mixture of P3OT and PCBM to form an interpenetrating bicontinuous network, resulting in low dark current (on the order of 10 $\mathrm{nA/cm}^2$) and high charge separation efficiency with responsivity up to 0.2 A/W. The spectral response of the image sensor was limited to visible wavelengths. A solution-processed F8T2 polymer-based phototransistor was also reported in 2004 [49], but the reported responsivity was limited to 0.7 mA/W.

A different approach, reported in 2004, was based on dye-sensitized photovoltaic photodetectors to address the near infrared [50]. The device consisted of a nanoporous TiO_2 layer infiltrated with various anionic dyes that acted as the light-absorbing material. The heterojunction was formed at the interface of the dye with TiO_2; upon illumination, the electrons were extracted through the TiO_2 and holes via a CuSCN overlayer used as a hole transport layer. The nanoporous TiO_2 was chosen to increase the interface area of the heterojunction, thereby leading to higher external quantum efficiency. The sensitivity of the device was extended from the visible to near infrared up to 950 nm. The reported responsivity was limited to $\sim$2 mA/W; the sensitivity of the device was reported as $D^* \sim 10^{10}$ Jones.

To overcome the carrier mobility bottleneck in conjugated polymers that limits their temporal response to several tens of microseconds, another class of flexible thin-film photodetectors has also been proposed [51]. These organic-based photodetectors consist of small organic molecule layers that have been evaporated onto ITO substrates; even though they lack solution processibility, they are promising for higher modulation frequency applications. The reported device consisted of alternating layers of CuPC and PTCBI to form a thin film of 32 nm in thickness. The resultant performance includes responsivity of 0.3 A/W, dark current on the order of 10^2 $\mathrm{nA/cm}^2$, and frequency response of $\sim$400 MHz.

The solution processibility and spectral tunability of colloidal quantum dots render them attractive for their application in photodetectors. Their compatibility with conjugated polymers allows for their integration to form nanocomposites with high interface area. These bulk heterojunctions provide high photon absorption and efficient exciton dissociation followed by charge separation. Upon illumination, excitons dissociate and electrons and holes

are transported to the contacts through separate paths within different physical media (polymer and nanocrystals), reducing recombination, and thereby increasing extraction efficiency.

A polymer-nanocrystal composite photodetector was reported in 1996 [52]. It consisted of a blend of CdSe or CdS nanocrystals mixed with MEH-PPV. This material system exhibits a type-II heterostructure wherein electrons are energetically favored to stay in the nanocrystals, whereas holes are transferred to the polymer matrix. The mixture was spin-coated on an ITO substrate, followed by metal evaporation to form the cathode. The efficiency of exciton dissociation was observed via the quenching of photoluminescence emitted by the nanocrystals. These devices were investigated as photovoltaic photodetectors. The reported quantum was ~12% at zero bias conditions, while it reached ~60% at 3 V. The spectral sensitivity of the reported device was limited by the absorption of MEH-PPV and Cd(S, Se) nanocrystals to the visible up to 650 nm.

A different approach based on neat colloidal nanocrystal films was reported in 2000 [53]. Photoconductivity in CdSe quantum dot solids was studied as function of applied electric field and nanocrystal surface passivation. In this device, photogenerated excitons are ionized by the electric field and dissociate into electrons and holes that hop amongst nanocrystals via either quantum dot bound states or surface trap states. In this approach, photocurrent competes with radiative and nonradiative recombination due to the fact that both types of carriers are transported via the same medium. The spectral sensitivity of this device was within the visible range, but absolute responsivity values were not reported.

Orders of magnitude increase in photoconductivity was reported [54] from this material system after postdeposition treatments of ligand exchange on the nanocrystal surface. It was found that shorter ligands were necessary to improve carrier transport among nanocrystals by decreasing internanoparticle spacing. The functionality of the ligand head group was also critical in order to passivate surface recombination states, prolonging thereby the carrier lifetime. Increasing exciton ionization efficiencies were also reported as a result of the ligand modification.

Our first contribution in the field was reported in 2005 [55], based on a polymer-nanocrystal bulk heterojunction device. This architecture is based on a photodiode principle of operation wherein photogenerated carriers are separated in two host media and transported to the respective contacts. The device structure is shown in Fig. 3. The active layer consists of a nanocomposite film of PbS nanocrystals in MEH-PPV polymer, sandwiched between a thin PPV buffer layer and the metal contacts.

MEH-PPV was chosen due to the high hole mobility and the favorable band offset with the PbS nanocrystals that forms a type-II heterostructure. This means that electrons favorably stay confined in the quantum dots, whereas holes are energetically favorable to tunnel to MEH-PPV. Upon photoexcitation, therefore, electron hole pairs created in the nanocrystals separate and electrons hop amongst nanocrystals to the anode, whereas holes are transported via the polymer towards the cathode. Under forward bias, electrons are extracted through the Mg contact and holes through the PPV/ITO contact. Even though this was the first demonstration of a solution-processed photodetector with infrared sensitivity from 1 to 1.5 μm, the responsivity of the diode is estimated on the order of 3 mA/W, prohibitively low for practical sensing applications.

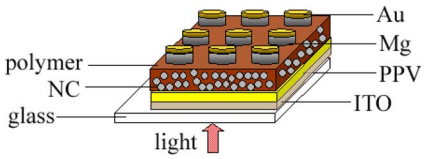

Fig. 3. *Device structure of the proposed solution processed photodiode based on MEH-PPV and PbS nanocrystals.*

To summarize: polymer photodetectors have previously been shown to demonstrate promising responsivities; however, their spectral sensitivity is limited to the visible range. Colloidal nanocrystal based photodetectors had previously been reported, but without a focus on the key figures of merit relevant to practical photodetection applications.

IV. SOLUTION-PROCESSED QUANTUM DOT PHOTOCONDUCTORS

A. SWIR Photodetection

In this section, we review our approach for sensitive solution-processed quantum dot photoconductive detectors based on PbS quantum dots for applications in the SWIR [56].

For sensitive photodetection, there are two prerequisite features: high photoconductive gain and low noise. Photoconductive gain expresses the number of electrical carriers circulated in the circuit per absorbed photon. This figure of merit determines the detector's ability to respond to light and is a crucial parameter for high sensitivity at a given noise level. The physical parameters that affect gain in a photoconductor are the minority carrier lifetime and the majority carrier transit time. For a sensitizing center characterized by a given carrier lifetime, therefore, increase in majority carrier mobility leads to higher photoconductive gains. Carrier transport in nanocrsytal solids takes place via a thermally activated hopping mechanism [57]. A determining parameter for the transport in these materials is the internanoparticle distance. The hopping probability depends exponentially on the internanoparticle spacing. High mobility thus mandates for nanocrystal close-packing [58].

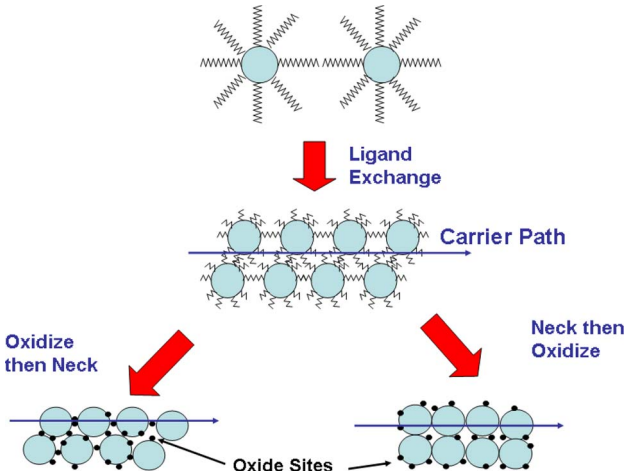

Fig. 4. *Material processing diagram for the development of SWIR photoconductive photodetectors.*

Increase in carrier lifetime in a photoconductor, also called photosensitization, can be achieved by introduction of sensitizing centers that trap one type of carrier but not the other. Previous studies in bulk PbS photoconductors have shown that photosensitization of PbS is followed by oxidation, and in particular formation of lead sulfates ($PbSO_4$) [59]–[62]. These oxide species act as sensitizing centers that prolong the minority (electron) carrier lifetime, allowing holes to transverse the device within this carrier lifetime.

Oleate-capped as-synthesized nanocrystals yielded films with insulating properties. The ∼2.5-nm-long ligand—consisting of an 18-carbon-atom chain—inhibited carrier transport among the nanocrystals. To improve carrier mobility, a postsynthetic ligand exchange process was employed to replace oleic acid with a shorter ligand attachable to the nanocrsytal Pb sites, leading to a decrease in the internanoparticle spacing. N-butylamine was, therefore, employed that consists of a four-carbon-atom chain of length ∼0.6 nm. The process is depicted in Fig. 4.

Photoconductive devices were fabricated by spin-coating butylamine exchanged nanocrystals to form a solid-state film on a prepatterned interdigitated gold electrode structure, as shown in Fig. 5(a). The active area of the detector is determined by the 3 mm length of the electrodes and their 5 μm gap spacing.

Further reduction of nanocrystal spacing is desirable in order to further increase mobility in these films and therefrom shorten the transit time of majority carriers. In order to detach any organic ligands from the nanocrystal surface and cause the nanocrystals to sinter, the devices, made of butylamine capped nanocrystals, were dipped in a methanol solution. Herein, this process is referred to as nanocrystal necking. Methanol is an aggressive nonsolvent for the nanoparticles, which, due to the high polarity, removes ligands from their surface.

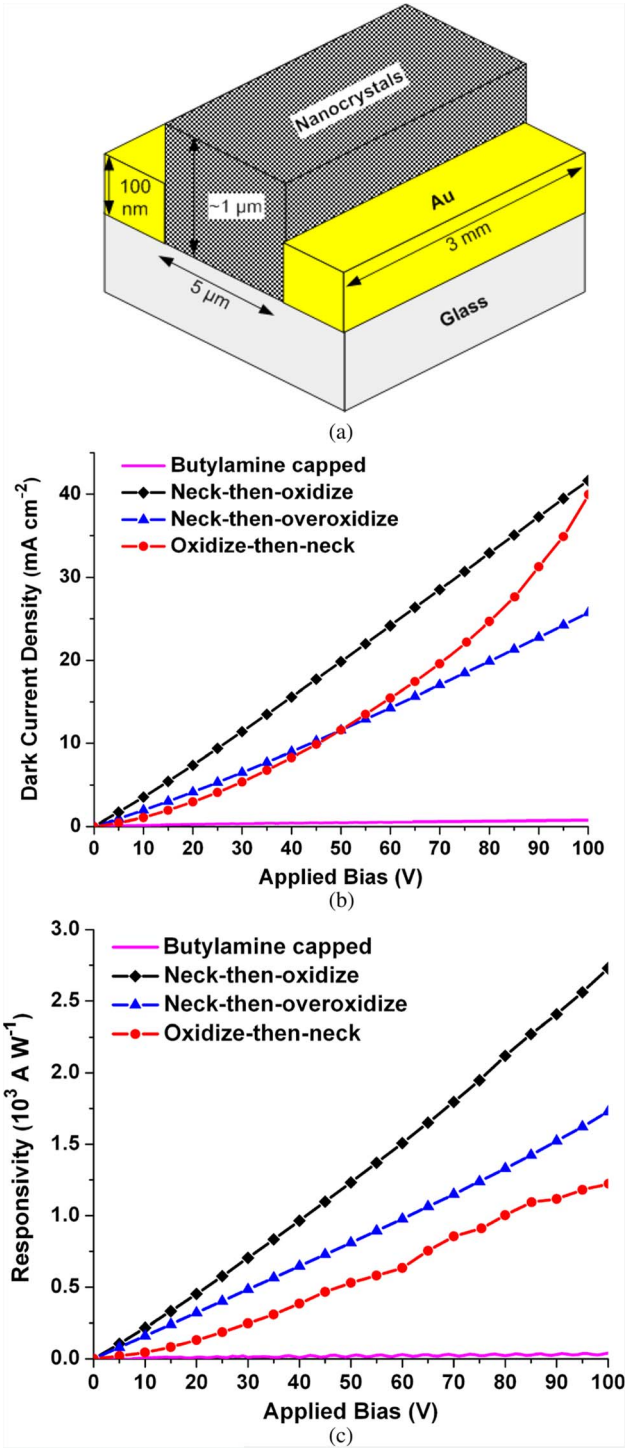

Fig. 5. *(a) Device structure of the colloidal quantum dot photoconductive photodetectors. (b) Dark current density as a function of applies bias of photoconductive devices. (c) Responsivity as a function of applied bias of photoconductive devices measured at a wavelength of 975 nm and light intensity of 300 nW/cm^2.*

Noise in photoconductors is determined by generation-recombination and shot noise. There have been reports, however, of excess noise, observed in polycrystalline

photoconductors [63], [64]. This excess noise is introduced by carrier transport along barriers formed at the interfaces of polycrystalline materials. These barriers that are randomly modulated by generation-recombination of thermal or photoexcited carriers cause excess noise superimposed to the shot and G-R noise components.

Material processing routes were developed that yield high carrier mobility and long carrier lifetime in order to achieve high photoconductive gain. This, however, must be achieved without compromising the noise performance of the device. We focused, therefore, on the effect of the sequence of the oxidation step on the noise current in order to minimize the excessive noise. The following four classes of devices were investigated along four process stages, as shown in Fig. 4.

1) *Butylamine capped:* Devices made of butylamine exchanged nanocrystals.
2) *Neck-then-oxidize:* Devices made of butylamine exchanged nanocrystals followed by necking using methanol treatment.
3) *Neck-then-over-oxidize:* Devices made as neck-then-oxidize followed by further oxidation by annealing the devices in ambient atmosphere at 120 °C.
4) *Oxidize-then-neck:* Devices made of butylamine exchanged nanocrystals that had been exposed to ambient conditions during the final steps of the ligand exchange so that oxidation takes place at this stage. The devices were then treated with methanol for necking.

Films made of nanocrystals as-synthesized, capped with oleic acid, were insulating due to the suppression of carrier transport by the long oleate ligand. After ligand exchange, the film exhibited measurable conductivity and the carrier density reached 0.73 mA/cm^2 at 100 V of bias. This is shown in Fig. 5(b). Responsivity of this device was also measured 27.7 A/W at 100 V, as shown in Fig. 5(c).

Further reduction of internanoparticle spacing via necking increased the dark current density to ~40 mA/cm^2 (a 57-fold increase) followed by an increase in responsivity of two orders of magnitude to 2700 A/W. The combined increase of both dark current density and gain following nanocrystal necking can therefore be attributed to an increase in mobility, since both dark and photocurrent are linearly related to mobility. Mobility increase, using MeOH and NaOH treatments, in CdSe nanocrystal films has also been reported [65]. To study the effect of the degree of oxidation on responsivity, the device was oxidized further by annealing in ambient conditions (neck-then-overoxidize). This led to a decrease in both responsivity and dark current density by a factor of ~1.6, which is suggestive of lower mobility.

The dark current–voltage characteristic indicates a field-activated transport mechanism when nanocrystals had been exposed to oxygen prior to film formation and necking (oxidize-then-neck). The superlinear behavior, shown in Fig. 5(b), is believed to result from carrier transport limited by potential barriers formed by the oxides. When oxidation takes place prior to film formation and necking, it leads to oxide barriers formed randomly on the nanocrystal surface. Upon necking, then, these potential barriers can be found at the points of nanocrystal necking along the carrier transport path (Fig. 4). In the case of neck-then-oxidize NCs, however, oxidation takes place at the exposed nanocrystal surface sites. It should be noted that in the case of oxidize-then-neck NCs, responsivity was as high as 10^3 A/W, lower by a factor of three compared to the neck-then-oxidize class of devices. The above findings suggest that the sequence of necking and oxidizing does not play a significant role in the responsivity performance of the photodetector.

A photodetector is ultimately characterized by its sensitivity. The noise current of the devices must be known in order to calculate the specific detectivity. The noise current was therefore measured to investigate the effects of oxidation and barrier formation on the noise performance. The sequence of oxidation and necking processes was also considered in the optimization of noise performance.

The measured noise current densities of the devices as a function of the dark current, which is the determinant factor of noise in photoconductors, are illustrated in Fig. 6(a). This representation allows comparison among devices with an eye to their deviation from the lower noise limit determined by the shot noise. Noise was measured at a modulation central frequency of 30 Hz, which is relevant to imaging applications.

By comparing the noise of the three classes of devices of butylamine capped, neck-then-overoxidize, and oxidize-then-neck, it is evident that electronic barriers contribute to high noise currents. The potential barriers in the butylamine-capped-nanocrystal case are due to the ligands, whereas in the other two cases, barriers are formed by the surface oxides. The oxidation step in the fabrication process is thus of critical importance in the noise performance of the device.

In order to present the best performing photoconductive device, responsivity and noise current should be jointly taken into account to yield specific (or normalized) detectivity D^*. Fig. 6(b) presents D^* of the devices described in the previous sections as a function of applied bias. The most sensitive device belongs to the neck-then-oxidize class of materials, whereas the less sensitive one is the device that had undergone oxidation prior to necking (oxidize-then-neck). The best performing device demonstrates a D^* on the order of 10^{13} Jones, which is roughly an order of magnitude higher than the best epitaxially grown InGaAs photodiodes [45].

The responsivity and resultant detectivity, as a function of wavelength, are illustrated in Fig. 7(a). The photocurrent spectrum follows the absorption spectrum of nanocrystals covering a broad wavelength range from ~1.5 μm towards the visible. The spectral response of the device is suited for

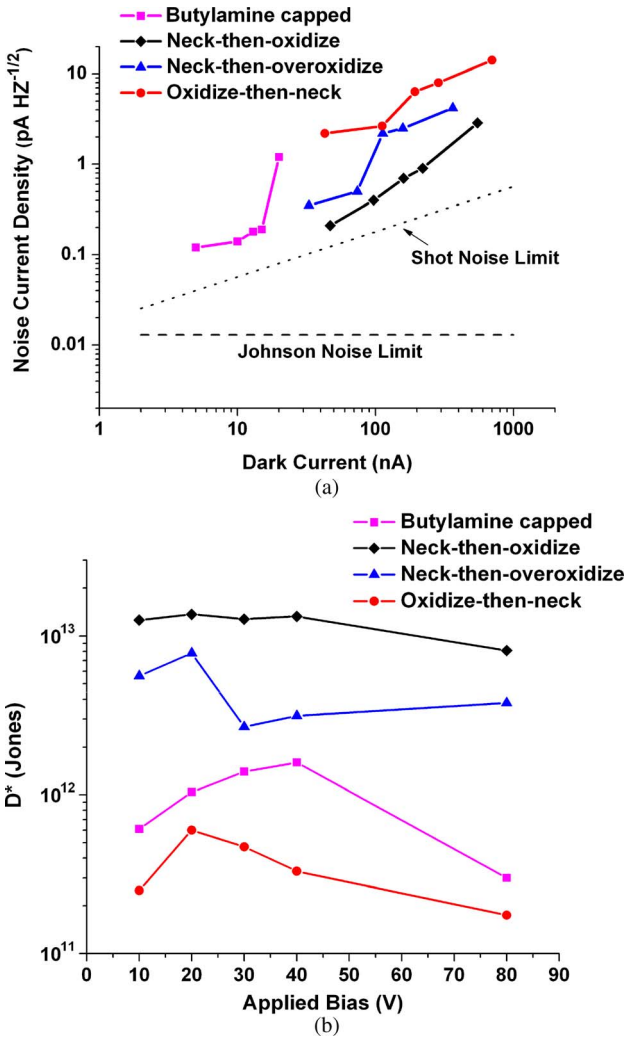

Fig. 6. *(a) Measured noise current as a function of measured dark current. The Johnson noise limit and the shot-noise limit of the best performing device (neck-then-oxidize) are also plotted for comparison. (b) Normalized detectivity* D^* *as a function of applied bias for the various classes of devices investigated herein.*

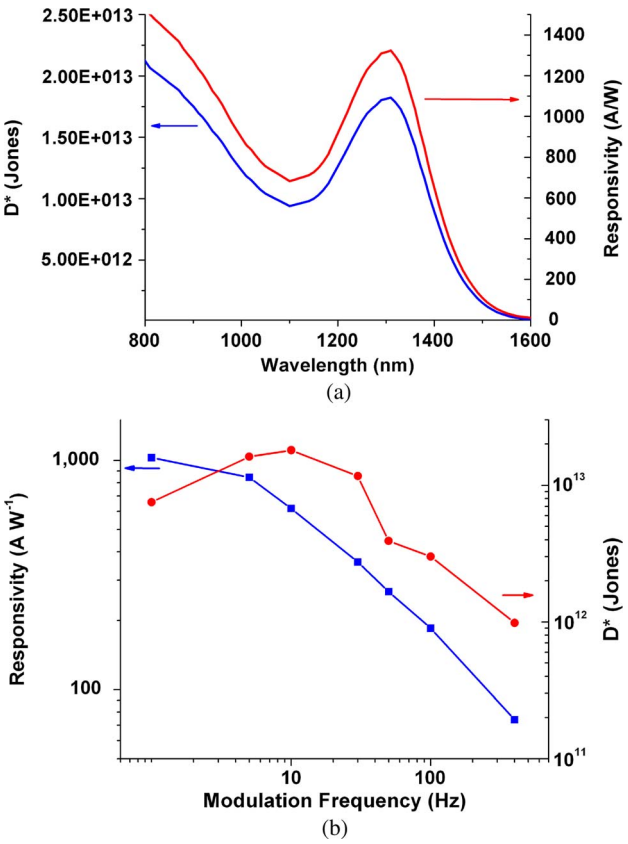

Fig. 7. *(a) Spectral responsivity and detectivity of the solution processed PbS quantum dot photodetector. (b) Responsivity and detectivity of the photodetector as a function of modulation frequency.*

night vision and biomedical imaging applications addressing the 800–1400 nm spectrum with high sensitivity of D^* greater than 10^{13} Jones. The responsivity and detectivity reported in Fig. 7(a) are taken with an applied electric field of 8 V/μm and modulation frequency of 30 Hz, relevant to imaging applications. The modulation frequency response is shown in Fig. 7(b), where responsivity is plotted as a function of modulation frequency considering an electric field of 8 V/μm and wavelength of 1300 nm. The device exhibits an effective 3-dB bandwidth of ~18 Hz. The temporal response of the device is limited by the minority carrier lifetime [41].

B. Visible and Multispectral Photodetection

The first sensitive solution-processed photodetector was described in the previous section. The device's performance in the infrared wavelengths relevant to night vision and biomedical imaging applications provided added utility and novelty. In contrast, sensing in the visible is central to mainstream imaging and video applications. The promising performance of the SWIR photodetector motivated the work of visible wavelength photodetection; the quantum size effect offered by quantum dots is exploited to demonstrate a visible solution-processed PbS colloidal quantum dot photoconductive detector.

The behavior of matter in the nanoscale imposed both opportunities and challenges that invalidated mere extrapolation of the existent material processing routes towards the development of visible-only PbS quantum dot photodetectors. These challenges are discussed herein, along with the solutions that led to a sensitive visible-wavelength solution-processed PbS quantum dot photodetector [66]. The solution processibility combined with spectral tunability, offered by colloidal quantum dots, is then exploited to demonstrate a multispectral photodetector promising for monolithic integration.

In view of PbS small (0.4 eV) bandgap, a very high degree of quantum confinement is required to make a visible-only photoconductive detector in this material

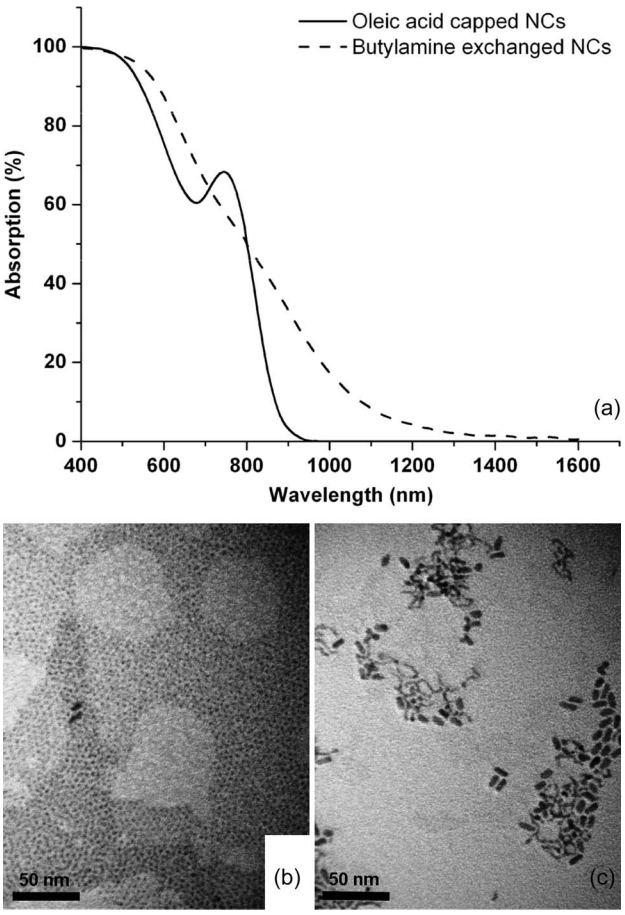

Fig. 8. *(a) Absorption spectra of PbS nanocrystals as-synthesized and after solution phase butylamine ligand exchange. (b) Transmission electron micrograph (TEM) of as-synthesized PbS nanocrystals. (c) TEM of solution phase butylamine ligand exchanged PbS nanocrystals.*

system. The synthetic procedure of previous reports was thus modified in order to synthesize small enough quantum dots so that their absorption onset would be below 800 nm [solid curve, Fig. 8(a)].

As synthesized, these nanocrystals were stabilized with oleic acid [Fig. 8(b)], a configuration shown above to inhibit carrier transport. Exchanging to shorter ligands such as butylamine was found above to produce a dramatic increase in conductivity. In the case of larger (4–6 nm in diameter) nanoparticles, monodispersity and excitonic features were preserved after ligand exchange in solution phase. In the small nanocrystal case, however, the procedure led, instead, to the formation of nanostrings [Fig. 8(c)] and, more deleteriously, a loss of an abrupt absorption onset [dashed curve, Fig. 8(a)] resulting from irreversible aggregation.

We sought an approach that would instead preserve a sharp, short-wavelength absorption onset to address selectively the visible part of the optical spectrum. We hypothesized that ligand exchange in the solid state, performed once thin films had already been formed, would limit the number of nanocrystal reattachment sites and improve conductivity without dramatically altering quantum-confined energy levels. PbS nanocrystals dispersed in toluene were spin-coated onto glass substrates with gold interdigitated electrodes with a 5 μm spacing to form a solid-state film. The optically active area of the detector is determined by the interelectrode distance (5 μm) and the electrode length (3 mm). The film was then treated in a mixture of butylamine in acetonitrile over two days in an inert nitrogen atmosphere.

Following this solid-phase ligand exchange, the film exhibited conductivity with dark current density 600 μA cm^{-2} at applied field of 20 V μm^{-1}. Fig. 9 exhibits spectral responsivity and normalized detectivity. The photoconductive gain reaches a maximum at wavelength 400 nm of ~113 A W^{-1} at 15 Hz. The quantum dot photodetector has an increasing responsivity at shorter wavelengths and optimal response in the visible part of spectrum. The electric field, required to achieve this gain, was 20 V μm^{-1}. The inset shows the noise equivalent power, which is the minimum power than can be detected by the detector with active area of 0.0015 mm^2, corresponding to a signal-to-noise ratio equal to unity.

The gain observed in sensitized photoconductors is due to sensitizing centers that prolong the carrier lifetime, which, in turn, determines the temporal response. This principle of operation influences the magnitude and temporal behavior of photoresponse with variation in the illumination level. The proportion of photoactivated sensitizing centers determines the effective responsivity and temporal response at a given optical intensity. Each sensitizing center has a specific energy depth that determines the lifetime and therefrom the gain. The number of occupied sensitizing centers therefore affects the total

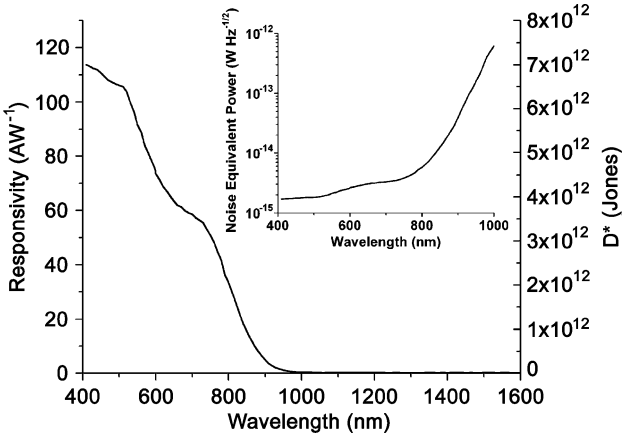

Fig. 9. *Spectral responsivity and normalized detectivity. The inset shows the spectral noise equivalent power for a device with active area of 0.015 mm^2.*

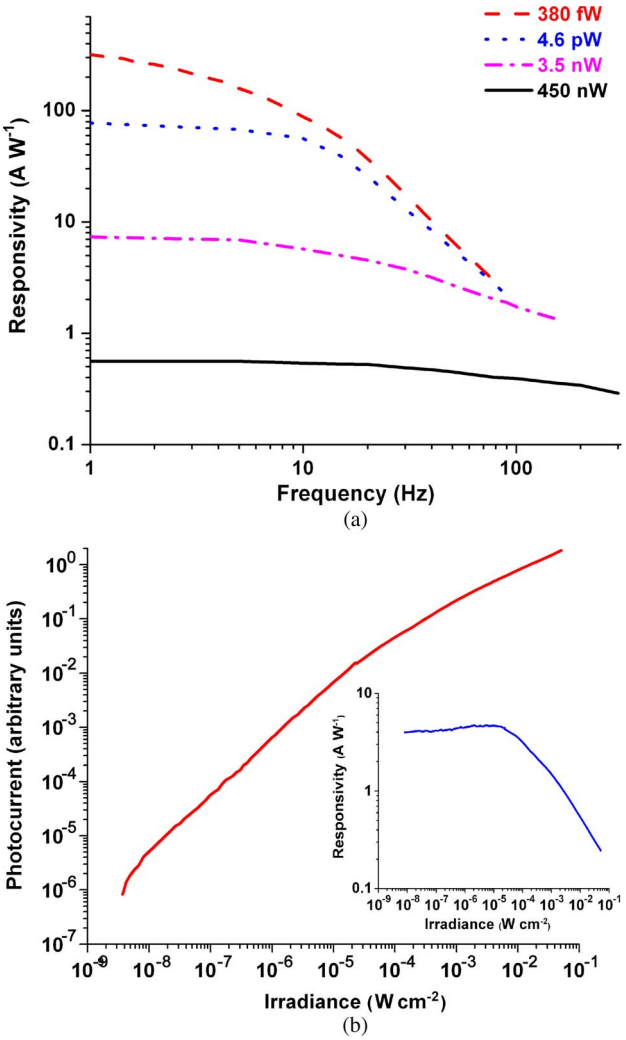

Fig. 10. *(a) Modulation frequency response of the detector at different impinging optical power levels at illumination wavelength of 630 nm. (b) The photocurrent plot versus optical illumination reveals a dynamic range of 7.5 orders of magnitude (conventionally expressed as 150 dB). The inset shows the responsivity as a function of optical intensity.*

responsivity and temporal response of the detector. The deeper trap states dominate the photoresponse at low optical intensities, resulting in slower temporal response and higher gain. Increasing illumination causes saturation of the deeper trap states followed by population of shallower centers. This reflects as an effective decrease of responsivity and acceleration of photocurrent decay with increasing illumination.

Further investigation of the effect of the trap states, in quantum dot photodetectors, on the optoelectronic characteristics of the device was then sought. In particular frequency response and responsivity, two features of practical interest, are measured at various optical intensities. Fig. 10(a) illustrates responsivity as a function of modulation frequency for a number of different optical power levels incident on the device. The decrease of responsivity with increasing optical power originates from filling of the lowest lying, longest lived trap states that provide the highest photoconductive gain at low intensities. As intensity increases, the effective responsivity drops as a result of increasing contribution in photocurrent from the shallower sensitizing centers with shorter lifetime. The 3-dB bandwidth increases from $\sim$8 Hz at 5 nW/cm^2 to $\sim$17 Hz at 60 nW/cm^2 and beyond 300 Hz at 6 mW/cm^2. The 3-dB bandwidth increase is followed by a two-order-of-magnitude decrease in responsivity. This phenomenon can provide the ability of a self-limiting gain mechanism to avoid electronic saturation at high optical power.

A significant figure of merit in photodetectors is dynamic range that expresses the intensity range within which the detector can distinguish among different optical intensities. Dynamic range is typically given as $20log(P_{max}/P_{min})$, where P_{max} is the maximum impinging power before saturation— a condition where photocurrent ceases to increase with increasing optical power; P_{min} is the minimum detectable optical power—or NEP.

In order to characterize the impact of high-gain trap state filling on the dynamic range of the detector, we measured the dependence of photocurrent on optical intensity at a modulation frequency of 30 Hz. We observed a monotonic, though at high intensities sublinear, dependence of photocurrent on intensity over more than 7.5 orders of magnitude in incident intensity corresponding to over 150 dB of intensity dynamic range [Fig. 10(b)]. The linear part of the curve extends for over three orders of magnitude corresponding to 60 dB of intensity linear dynamic range, which is what typically is required for most imaging applications. At higher optical intensities, however, the detector exhibits an inherent sublinear transformation of the optical signal to electrical output desired for increased intrascene dynamic range [67]. The inset of Fig. 10(b) shows the onset of responsivity decrease, which is due to the filling of the high-gain trap states at higher intensities.

In the previous section, a sensitive solution-processed PbS quantum dot photodetector was developed to address the short wavelength and near infrared part of the spectrum, preserving, however, its sensitivity also in the visible. In the current section, a solution-processed PbS quantum dot photodetector was presented, the absorption of which was tailored to address the visible part of spectrum.

The superiority of solution processibility is demonstrated herein by combining the two classes of photodetectors to compose a dual-spectral photodetector that can sense light from 1500 to 400 nm in a broadband or selective mode of operation. This was achieved based on the same material of PbS quantum dots. The inset of Fig. 11 shows the photodetector architecture that demonstrated dual-spectral detection. The device consists of two stacked PbS quantum dot photodetectors of different nanocrystal size. The top

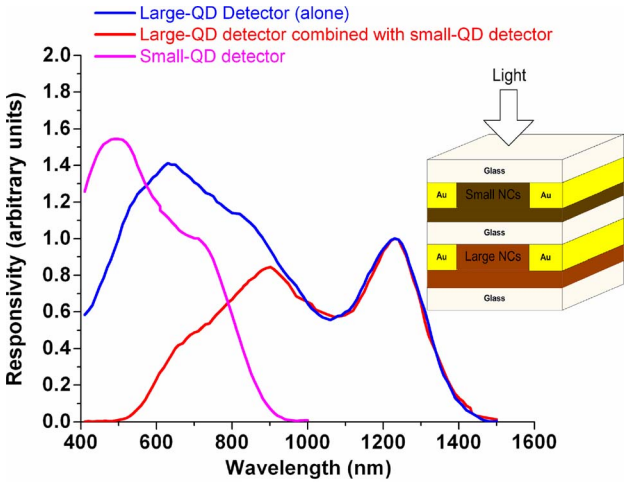

Fig. 11. ***Spectral responsivity of the stacked device shown in the inset for dual-spectral detection. The small quantum dot (QD) layer detects effectively the short wavelength light, whereas the longer wavelengths are detected from the large QD layer. The responsivity of the large QD device before the stacking is also shown for comparison.***

detector is fabricated by small PbS quantum dots that detect effectively in the visible part of spectrum. The buried photodetector consists of larger PbS quantum dots to detect light in the SWIR and near infrared. This layer, however, is prone to detecting light in the visible. The top layer then serves not only as a photosensitive layer of the visible but also as a filter to prevent visible photons from reaching the second layer. The sensitivity of the buried photodetector is thus suppressed in the visible part of spectrum.

The resultant responsivity spectra of the photodetectors are shown in Fig. 11. The responsivities of the large quantum dot device in both cases have been normalized to their exciton peak value at 1230 nm. The large photodetector in the stacked structure preserves responsivity at wavelengths longer than 900 nm, which demonstrates significant decrease in responsivity at shorter wavelengths following the absorption onset of the small quantum dot photodetector. The spectral responsivity of the small-bandgap detector prior to stacking is also shown to demonstrate the achieved suppression of responsivity in the visible by over 20 dB at 500 nm and beyond.

C. Trap-State Engineering Towards Video Frame Rate Applications

In the previous sections, we demonstrated the first achievement of highly sensitive photodetection in each of the visible and the infrared based on solution-processed materials. This was achieved by sensitizing colloidal quantum dots using surface trap states such as to prolong the carrier lifetime. Photoconductive gain, responsible for high sensitivity, is given by τ_c/τ_t, where τ_t is the time for the flowing carrier to transit the extent of the device and τ_c is the carrier lifetime [40]. From a sensitivity point of view alone, this argues for longer trap-state lifetimes.

Also important in photodetection is temporal response. If the response of a photodetector to an optical transient exceeds the frame period, then lag, or ghosting, will be perceptible in the image. Conventional imaging applications typically require frame rates in the range of 10, 15, 30, or 60 frames per second. Temporal responses having time constants in the range of tens of milliseconds are thus required. The temporal response is directly determined by the carrier lifetime. The challenge of practical photoconductive photodetector design is thus to establish a suitable balance between gain and temporal response and to control material composition with care to implement the resultant design.

The energy levels associated with trap states in PbS colloidal quantum dot photodetectors that exhibit gains on the order of 100 A/W were investigated using responsivity quenching and transient photocurrent spectroscopy [68]. Three sensitizing centers at 0.1, 0.2, and 0.34 eV from the conduction band resulted in carrier lifetimes of ~60, 300, and 2000 ms. Although the shortest lifetime of 30 ms is suited for many imaging applications, the longer ones, which dominate at lower optical intensities in view of their deeper energy levels, introduce unacceptable lag.

In this section, we present our approach on the correlation between the oxide species existent on the quantum dot surface and the resultant sensitizing centers with measured time constants and their related trap-state energies [69]. This study led to a novel material-processing methodology that facilitates suppression of the longest lived trap states. In so doing, we preserve sensitization only via the shortest (temporally), thus the shallowest (energetically), trap state. As a result, we report the first solution-processed photoconductive photodetector to combine application-relevant temporal response with superb sensitivity.

For the purpose of the study reported in this paper, photoconductive devices made of nanocrystals with ligands of various head functional groups attaching to nanocrystal surface are fabricated. Three types of ligands with different functional groups were employed: butylamine treated nanocrystals, formic acid treated nanocrystals, and ethanethiol treated nanocrystals.

The correlation study between nanocrystal surface species and temporal response begins with butylamine treated nanocrystal devices. These devices demonstrate multiple photocurrent decay time constants of ~60, 300, and 2000 ms at room temperature (Fig. 12). X-ray photoelectron spectroscopy (XPS) analysis of nanocrystal treated using butylamine revealed the presence of lead sulfate ($PbSO_4$), lead sulfite ($PbSO_3$), and lead carboxylate attributable to oleic acid ligands attached to the nanoparticles' surfaces. The number of species found on the nanocrystal surface ($PbSO_4$, $PbSO_3$, and Pb-carboxylate) is equal to the

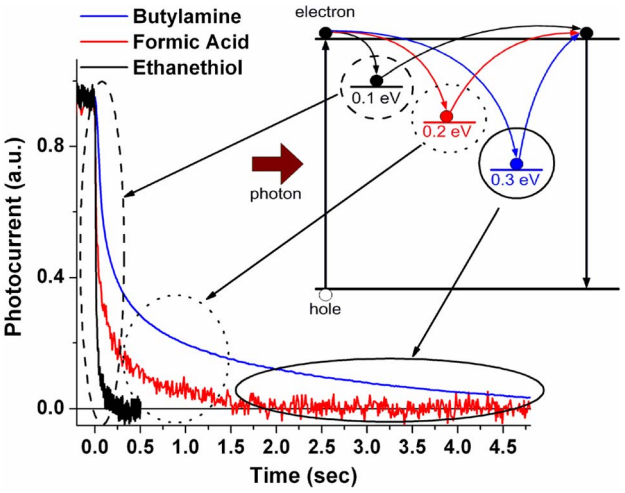

Fig. 12. *Temporal response of photocurrent in butylamine, formic acid, and ethanethiol treated nanocrystal films. The inset shows the associated trap state levels responsible for the corresponding temporal components of the photocurrent.*

number of photocurrent decay time constants; this is suggestive that each of the identified species is responsible for a single time constant, associated with the energy depth of the trap.

The correlation between the lead carboxylate peak (due to the oleic acid-Pb bond) and a corresponding sensitizing trap state, having a specific temporal response, is initially addressed. Nanocrystal films were treated with formic acid to exchange the long oleic acid ligand with a shorter one, preserving the carboxylic functionality to prevent sulfate formation. In so doing, the internanoparticle spacing was reduced while preserving the carboxylate moiety bound to Pb atoms on the nanocrystal surface. In this way, insulating devices were transformed into photoconductive detectors. Temporal measurements of photocurrent response revealed a main time constant of ~420 ms (Fig. 12) and also a faster component with time constant ~33 ms. XPS, in this case, revealed the presence of Pb-carboxylate group as well as $PbSO_3$. This evidence suggests that either Pb-carboxylate or $PbSO_3$ serves as a sensitizing species having an (undesirably long-lived) ~420 ms time constant.

Complete removal of the oleate ligands was sought in order to unmask which among the carboxylate/sulfite species is responsible for the ~420 ms time constant. A ligand, short enough to promote transport and lacking carboxylate functionality, is needed. To make the replacement of the carboxylate-terminated ligand thermodynamically favorable, a functional head-group that would bind to the Pb more strongly than Pb-carboxylate was also required. Ethanethiol was chosen for its short length and its thiol moiety, expected to bind strongly with Pb. Photoconductive devices were thus fabricated from thiol-treated nanocrystals. XPS confirmed the complete removal of Pb-carboxylate following ethenethiol treatment, leaving $PbSO_3$ as the sole oxidized species. Transient photocurrent measurements showed that ethanethiol treated nanocrystal films exhibited a single transient component having a ~27 ms time constant at room temperature (Fig. 12). These optimized devices demonstrated photoconductive gains on the order of 10 A/W under electric field of 2 V/μm and normalized detectivity of 10^{12} Jones across the visible [69].

V. SOLUTION-PROCESSED QUANTUM DOT PHOTODIODES

We showed in the previous section that colloidal quantum dot photoconductive photodetectors may yield sensitivities up to 10^{13} Jones. These remarkable sensitivities resulted from high photoconductive gain and low noise current. Photoconductive gain, however, requires carrier lifetimes that limit the temporal response of the devices to a few tens of milliseconds. Therefore, applications requiring high modulation frequencies such as machine vision, high-speed process monitoring, and optical communications are not generally addressed by this approach. Emerging classes of photodetectors, for these applications, must demonstrate both high sensitivity and high response speed if they are to compete in performance with photodetectors fabricated from traditional crystalline semiconductors.

An alternative to photoconductors approach, the photodiode, is therefore explored in this section. Prior to this work [70], there had been no previous reports of colloidal quantum dot photodiodes that can achieve simultaneously high speed and sensitivity. The first report of a fast colloidal quantum dot detector (50 kHz bandwidth) demonstrated sensitivity in the visible with estimated $D^* \sim 10^8$ Jones [71]. This device, a diode formed by the metallurgical junction between CdSe nanocrystals and a conductive polymer, had a zero-bias EQE of ~0.15% at the first excitonic wavelength of ~560 nm.

Considering a Schottky-barrier type photodiode formed between the nanocrystal film and a metal, we recognized that efficient carrier transport and metallurgical junction with a large built-in potential could potentially lead to the desired combination of sensitivity and speed. Nanocrystal films provide a number of chemically tunable degrees of freedom, which control their macroscopic electronic properties. The spacing between individual nanocrystals is controlled by the length of the organic ligands used to passivate their surfaces. This has been shown to be a determinant factor of the carrier mobility. The consistency of surface passivation is also important, as it limits oxidation and other chemical modification of the nanocrystal surface. Oxidation provides a path to nanocrystal doping; however, uncontrolled surface variation leads to interface states and a reduction

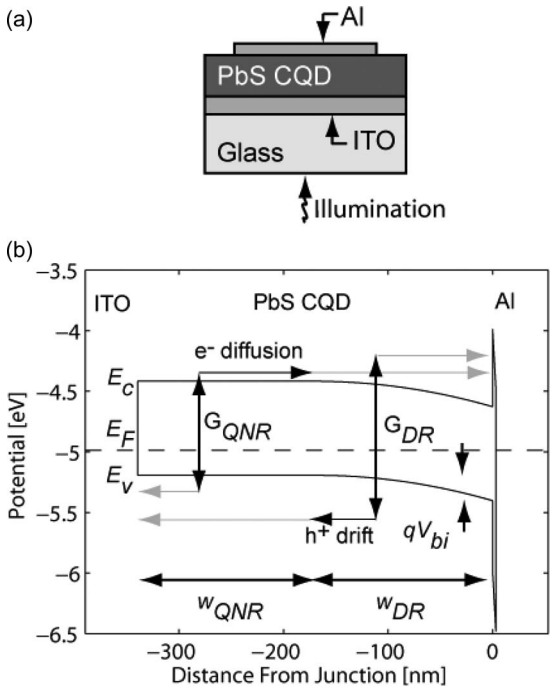

Fig. 13. *(a) A schematic representation of the photodiode device architecture. (b) Band diagram of the device demonstrating the Schottky barrier at the Al/PbS nanocrystal interface.*

of the built-in potential. Noise performance in diodes is determined by the shunt resistance, which in turn depends on the energetic barrier associated with the metallurgical junction. Thus, this interfacial control is essential for fabricating high-sensitivity photodiodes. Colloidal nanocrystals provide access and control of their surface properties via careful choice of the passivating ligands yielding simultaneously high mobilities and lack of surface states.

Photodiodes were formed between PbS nanocrystal film and an aluminum contact [Fig. 13(a)]. A planar transparent ITO thin film formed the opposing ohmic contact. Light incident through the glass substrate generates electrons and holes in CQD film that are collected at the Al and ITO contacts, respectively. The energy band diagram in Fig. 13(b) shows the Schottky barrier formed at the Al/PbS CQD interface and the built-in potential derived from the difference in work function between the nanocrystals and the metal contact [72]. Charge transfer between the semiconductor and the metal results in the formation of a wide depletion region in the nanocrystal film, while the remaining volume of the film is a quasi-neutral region of p-type semiconductor with no net charge or electric field. The formation of Schottky barrier limits majority carrier (hole) injection from the Al contact, resulting in highly rectifying dark I–V characteristics [72].

For the study reported in this paper, PbS colloidal quantum dots were synthesized with diameter of ~6 nm and first excitonic absorption feature at 1450 nm in order to address both the visible and SWIR spectra.

Due to the insulating properties of oleic acid, the capping molecule of as-synthesized nanocrystals, we followed a ligand exchange to replace it with short butylamine ligands. The lack of stability of amines with respect to PbS nanocrystal forming consistent Schottky barrier with aluminum led us to employ a bidendate linker molecule that would instead utilize a much stronger binding interaction with PbS nanocrystals providing higher stability [73] and preserving at the same time the close-packing of nanocrystals. Benzenedithiol (BDT) was used for this purpose.

It was found, however, that BDT's thiol endgroup chemically reduces the surface of PbS nanocrystals by removing oxidation species that are known to act as p-type dopants. This reduction suppresses the effective doping and p-type semiconductor characteristics and thus diminishes the built-in potential of the Schottky barrier from which diode behavior originates. At the final stage, a reoxidation of the nanocrystal film was performed to return the degree of effective doping required for creating Schottky barriers with a large built-in potential and energy barrier.

The EQE (at 295 K) and normalized detectivity (at 250 K) as a function of wavelength are plotted in Fig. 14. An EQE of 17% is achieved at 1450 nm and reaches a maximum of 52% at 580 nm. D^* is on the order of 10^{11} Jones at 1450 nm, at room temperature, whereas it increases to order of 10^{12} Jones for temperatures below 255 K. This dramatic improvement over previous reports of colloidal quantum dot photodiodes results from the large built-in potential of 0.2 V that improves the photogenerated charge separation efficiency.

The temporal decay of the photocurrent is illustrated in Fig. 15(a) to demonstrate the superior performance of the photodiode's temporal response. The 3 dB frequency is 10.7 kHz at zero bias and 1.95 μW/cm^2. At each bias,

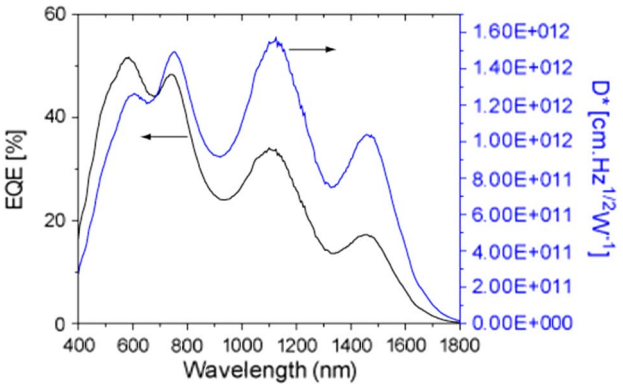

Fig. 14. *External quantum efficiency (at 295 K) and normalized detectivity (at 250 K) as a function of wavelength.*

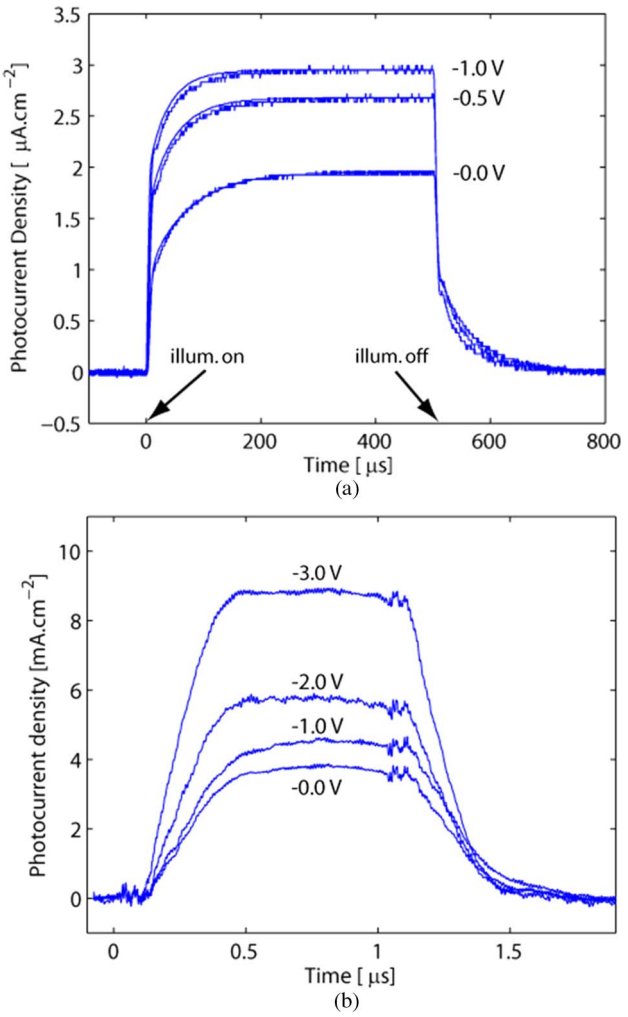

Fig. 15. *(a) Photocurrent transient response of the partially depleted diode, as a function of bias, to a 500 μs square illumination pulse at 17.9 μW/cm^2 at 1550 nm. (b) Photocurrent transient response of the partially depleted diode as a function of bias to a 1 μs square illumination pulse at 40 mW/cm^2 at 1550 nm.*

the transient response is composed of two distinct components—an initial, fast, component linearly increasing with bias and a slower component that exponentially settles to a steady state. These temporal components correspond to the time required to reach the steady state in the quasi-neutral region and the transit time of the depletion region ~500 μs and ~10 μs, respectively, as shown in Fig. 15(a). The fast photocurrent component is attributed to carriers generated in the depletion region and quickly swept out by a drift current proportional to the built-in electric field. The slower component is attributed to electrons generated in the quasi-neutral region, which must diffuse to the depletion region before they are effectively swept out by the built-in electric field. The rise time of this component is the time required for generation, diffusion, and recombination processes in the quasi-neutral region to reach a steady state and is dependent on the width of the quasi-neutral region (w_{QNR}) and inversely dependent on the electron diffusion coefficient (D_e).

These findings pointed toward the following hypothesis: an efficient and much faster photodiode could be developed if the sole mechanism of carrier transport were due to drift. In a fully depleted photodiode, all photogenerated electrons and holes are swept directly to the contacts by the electric field from the built-in potential of the junction and any externally applied bias. A fully depleted was developed by reducing the thickness of the film to match the depletion region width (180 nm). This resulted in the appearance of a single temporal component of photocurrent limited only by the drift transit time (~300 ns), as illustrated in Fig. 15(b). The flatness of the frequency response of the fully depleted photodiode extends beyond 100 kHz and the 3-dB frequency of this device ranges from 1.6 MHz at zero bias to $>$ 2.9 MHz at -5 V bias. The increase in operating speed with applied

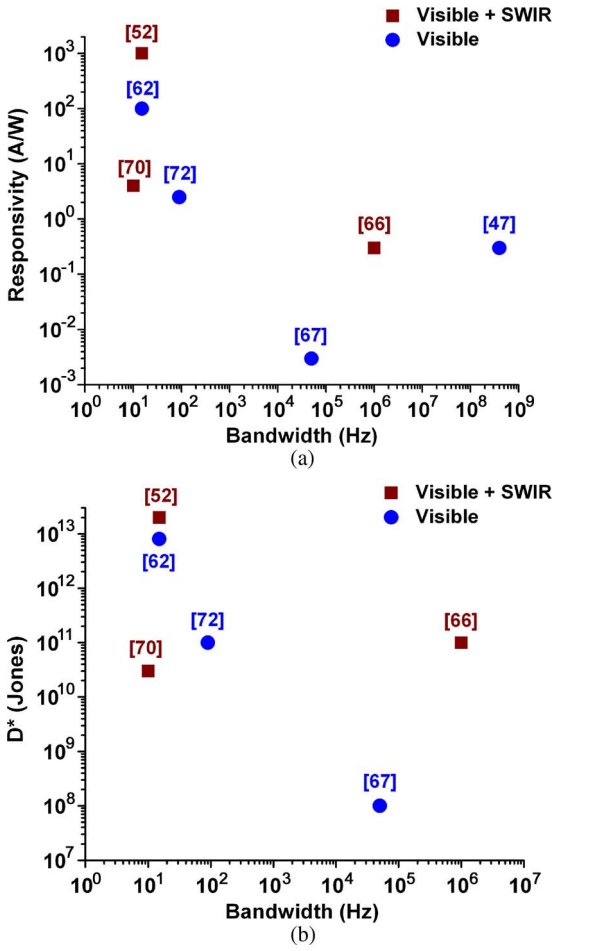

Fig. 16. *Current progress of solution-processed photodetectors. (a) Responsivity-bandwidth dependence and (b) Normalized detectivity-bandwidth dependence of the reported technologies based on solution-processed thin-film photodetectors.*

bias is due to the reduction in carrier transit time with increasing electric field in the depletion region. By further optimization of the material for higher carrier mobility the ultimate normalized detectivity of the fast device was preserved on the order of 10^{11} Jones at room temperature, representing the best performing solution processed photodiode combining high sensitivity and megahertz frequency response.

VI. CONCLUSION

Solution-processed optoelectronic materials such as colloidal quantum dots offer dramatically lowered manufacturing cost and ease of large-area fabrication, including on flexible substrates. Significant further advantages in an imaging context include high pixel count and small pixel size; outstanding sensitivity, including gain, reported herein; and access to new spectral regimes and multispectral capabilities outside silicon's realm.

Control over material definition on the nanoscale also enables for device functionalities impossible to achieve with conventionally grown semiconductors. Device physics and performance in colloidal nanocrystal devices, unlike bulk semiconductors, are determined by the nanocrystal surface and size. These two factors can readily be tuned via wet chemistry to tailor the material properties: the absorption and emission spectra can be tailored by choice of the nanocrystal size; mobility may be controlled through the length of the capping ligands and nanocrystal size, shape, and ordering; carrier doping can be transformed between n-type and p-type by surface modification; carrier lifetime, determined by surface traps, can be tuned via selective passivation of the nanocrystal surface trap states.

This paper showcases the high degree of control offered by nanoscale materials engineering.

- High mobilities were achieved, via control of the nanocrsytal spacing and surface passivation, essential to photoconductive gain in photoconductors and to high EQE and frequency response in photodiodes.
- Control over surface passivation enabled stable Schottky barriers for high extraction efficiency in photodiodes and sensitizing centers that prolong carrier lifetimes in photoconductors and enable manipulation for fine-tuning of their temporal response.
- Spectral tunability via the quantum size effect permitted optimized spectral matching of the photodetector to the addressed application for minimum generation-recombination noise and development of monolithic multispectral photodetectors.

Further progress has also been made in solution-processed nanocrystalline photodetectors towards expansion of spectral sensitivity in the midwavelength infrared up to 3 μm using HgTe nanocrystals [74] and into the ultraviolet using visible-blind ZnO quantum dot photodetectors [75]. Their convenient integration into large-area flexible arrays has been demonstrated [76]. Another emerging field of research is the exploration of candidate materials for sensitive photodetection that do not contain heavy metals. Bi_2S_3 nanocrystalline sensitive photodetectors in the visible part of spectrum have recently been reported [77]. Novel material processes have been demonstrated to achieve very low spatial nonuniformity of response essential to large-area imaging applications [78]. Colloidal quantum dot photodetectors have also been reported as a candidate material for near-field imaging applications [79].

In Fig. 16, we summarize the performance of the reported sensitivities from solution-processed photodetectors addressing the two main spectral windows of interest: visible and SWIR. Photoconductive photodetectors demonstrate high photoconductive gains but frequency response typically in the tens of hertz. This behavior renders them suitable for most imaging applications with consumer-oriented video frame rates. Photodiodes, on the other hand, offer attractive bandwidths in the megahertz. We believe that this young field, though its pace of recent progress has been impressive, holds further potential in the optimization of sensitivity and speed. ■

Acknowledgment

The authors would like to thank J. P. Clifford, L. Levina, S. Hinds, S. McDonald, A. Fischer, S. Hoogland, I. Howard, E. Klem, and K. Johnston for their contributions in the work reviewed herein.

REFERENCES

[1] L. M. Vatsia, "Atmospheric optical environment," Research and Development Tech. Rep. ECOM-7023, 1972.

[2] M. Ettenberg, "A little night vision," *Adv. Imag.*, vol. 20, pp. 29–32, 2005.

[3] X. Gao, Y. Cui, R. M. Levenson, L. W. K. Chung, and S. Nie, "In vivo cancer targeting and imaging with semiconductor quantum dots," *Nature Biotechnol.*, vol. 22, no. 18, pp. 969–976, 2004.

[4] Y. T. Lim, S. Kim, A. Nakayama, N. E. Stott, M. G. Bawendi, and J. F. Frangioni, "Selection of quantum dot wavelengths for biomedical assays and imaging," *Molec. Imag.*, vol. 2, pp. 50–64, 2003.

[5] S. Kim, Y. T. Lim, E. G. Soltesz, A. M. De Grand, J. Lee, A. Nakayama, J. A. Parker, T. Mihaljevic, R. G. Laurence, D. M. Dor, L. H. Cohn, M. G. Bawendi, and J. V. Frangioni, "Near-infrared fluorescent type II quantum dots for sentinel lymph node mapping," *Nature Biotechnol.*, vol. 22, pp. 93–97, 2004.

[6] R. Schödel, T. Ott, R. Genzel, R. Hofmann, M. Lehnert, A. Eckart, N. Mouawad, T. Alexander, M. J. Reid, R. Lenzen, M. Hartung, F. Lacombe, D. Rouan, E. Gendron, G. Rousset, A.-M. Lagrange, W. Brandner, N. Ageorges, C. Lidman, A. F. M. Moorwood, J. Spyromilio, N. Hubin, and K. M. Menten, "A star in a 15.2-year orbit around the supermassive black hole at the centre of the Milky Way," *Nature*, vol. 419, pp. 694–696, 2002.

[7] W. Herrmann, M. Blake, M. Doyle, D. Huston, J. Kamprad, N. Merry, and S. Pontual, "Short wavelength infrared (SWIR) spectral analysis of hydrothermal alteration zones associated with base metal sulfide deposits at Rosebery and Western Tharsis, Tasmania, and Highway-Reward, Queensland," *Econ. Geol.*, vol. 96, pp. 939–955, 2001.

[8] M. Golic, K. Walsh, and P. Lawson, "Short-wavelength near-infrared spectra of sucrose, glucose, and fructose with respect to sugar concentration and temperature," *Appl. Spectrosc.*, vol. 57, no. 2, pp. 64A–85A and 117–243, 2003.

[9] J. Kang, A. Borkar, A. Yeung, N. Nong, M. Smith, and M. Hayes, "Short wavelength infrared face recognition for personalization," in *Proc. IEEE Int. Conf. Image Process.*, Oct. 8–11, 2006, pp. 2757–2760.

[10] T. Hoetler, "Broad spectrum performance via VisGaAs," *Adv. Imag.*, vol. 18, pp. 14–19, 2003.

[11] J. Nakamura, *Image Sensors and Signal Processing for Digital Still Cameras*. Boca Raton, FL: Taylor & Francis/CRC Press, 2006.

[12] E. R. Fossum, "CMOS image sensors: Electronic camera-on-a-chip," *IEEE Trans. Electron Devices*, vol. 44, pp. 1689–1698, 1997.

[13] J. A. Theil, "a-Si:H photodiode technology for advanced CMOS active pixel sensor imagers," *J. Non-Crystal. Solids*, vol. 299–302, pp. 1234–1239, 2002.

[14] Y. Vygranenko, J. H. Chang, and A. Nathan, "Two-dimensional a-Si:H n-i-p photodiode array for low-level light detection," *IEEE J. Quantum Electron.*, vol. 41, pp. 697–703, 2005.

[15] D. L. Staebler and C. R. Wronski, "Reversible conductivity changes in discharge-produced amorphous Si," *Appl. Phys. Lett.*, vol. 31, pp. 292–294, 1977.

[16] P. P. Web, R. J. McIntyre, and J. Conradi, "Properties of avalanche photodiodes," *RCA Rev.*, vol. 35, pp. 235–278, 1974.

[17] A. Biber, P. Seitz, and H. Jackel, "Avalanche photodiode image sensor in standard BiCMOS technology," *IEEE Trans. Electron Devices*, vol. 47, pp. 2241–2243, 2000.

[18] J. C. Campbell and A. Mdhukar, "Quantum dot infrared photodetectors," *Proc. IEEE*, vol. 95, no. 9, pp. 1815–1827, 2007.

[19] S. Krishna, S. D. Gunapala, S. V. Bandara, C. Hill, and D. Z. Ting, "Quantum dot based infrared focal plane arrays," *Proc. IEEE*, vol. 95, no. 9, pp. 1838–1852, 2007.

[20] P. Bhattacharya, X. Su, G. Ariyawansa, and G. U. Perera, "High temperature tunneling quantum-dot intersublevel detectors for mid-infrared to terahertz frequencies," *Proc. IEEE*, vol. 95, no. 9, pp. 1828–1837, 2007.

[21] P. Bhattacharya and Z. Mi, "Quantum-dot optoelectronic devices," *Proc. IEEE*, vol. 95, no. 9, pp. 1723–1740, 2007.

[22] S. B. Samavedam, M. T. Currie, T. A. Langdo, and E. A. Fitzgerald, "High-quality germanium photodiodes integrated on silicon substrates using optimized relaxed graded buffers," *Appl. Phys. Lett.*, vol. 73, pp. 2125–2127, 1998.

[23] O. Qasaimeh, Z. Ma, P. Bhattacharya, and E. T. Croke, "Monolithically integrated multichannel SiGe/Si p-i-n-HBT photoreceiver arrays," *J. Lightw. Technol.*, vol. 18, pp. 1548–1553, 2000.

[24] L. Colace, G. Masini, S. Cozza, G. Assanto, F. DeNotaristefani, and V. Cencelli, "Near-infrared camera in polycrystalline germanium integrated on complementary metal oxide semiconductor electronics," *Appl. Phys. Lett.*, vol. 90, p. 011103, 2007.

[25] S. Coe, W. K. Woo, M. Bawendi, and V. Bulovic, "Electroluminescence from single monolayers of nanocrystals in molecular organic devices," *Nature*, vol. 420, pp. 800–803, 2002.

[26] G. Konstantatos, C. Huang, L. Levina, Z. Lu, and E. H. Sargent, "Efficient infrared electroluminescent devices using solution-processed colloidal quantum dots," *Adv. Funct. Mater.*, vol. 15, pp. 1865–1869, 2005.

[27] S. Hoogland, V. Sukhovatkin, I. Howard, S. Cauchi, L. Levina, and E. H. Sargent, "A solution-processed 1.53 um quantum dot laser with temperature-invariant emission wavelength," *Opt. Express*, vol. 14, pp. 3273–3281, 2006.

[28] E. J. D. Klem, L. Levina, and E. H. Sargent, "PbS quantum dot electroabsorption modulation across the extended communications band 1200-1700 nm," *Appl. Phys. Lett.*, vol. 87, p. 053101, 2005.

[29] S. A. McDonald, G. Konstantatos, S. Zhang, P. W. Cyr, E. J. D. Klem, L. Levina, and E. H. Sargent, "Solution-processed PbS quantum dot infrared photodetectors and photovoltaics," *Nature Mater.*, vol. 4, no. 2, pp. 138–142, 2005.

[30] I. Gur, N. A. Fromer, M. L. Geier, and A. P. Alivisatos, "Air-stable all-inorganic nanocrystal solar cells processed from solution," *Science*, vol. 310, pp. 462–465, 2005.

[31] S. A. McDonald, P. W. Cyr, L. Levina, and E. H. Sargent, "Photoconductivity from PbS nanocrystal/MEH-PPV composites for solution-processible, quantum-size tunable infrared photodetectors," *Appl. Phys. Lett.*, vol. 85, pp. 2089–2091, 2004.

[32] A. L. Efros and M. Rosen, "The electronic structure of semiconductor nanocrystals," *Annu. Rev. Mater. Sci.*, vol. 30, pp. 475–521, 2000.

[33] B. Crone, A. Dodabalapur, Y. Y. Lin, R. W. Filas, Z. Bao, A. Laduca, R. Sarpeshkar, H. E. Katz, and W. Li, "Large-scale complementary integrated circuits based on organic transistors," *Nature*, vol. 403, pp. 521–523, 2000.

[34] T. Someya, T. Sekitani, S. Iba, Y. Kato, H. Kawaguchi, and T. Sakurai, "A large-area, flexible pressure sensor matrix with organic field-effect transistors for artificial skin applications," *Proc. Nat. Acad. Sci.*, vol. 101, pp. 9966–9970, 2004.

[35] T. Someya, Y. Kato, S. Iba, Y. Noguchi, T. Sekitani, H. Kawaguchi, and T. Sakurai, "Integration of organic FETs with organic photodiodes for a large area, flexible, and lightweight sheet image scanners," *IEEE Trans. Electron Devices*, vol. 52, pp. 2502–2511, 2005.

[36] I. Kymissis, A. I. Akinwande, and V. Bulovic, "A lithographic process for integrated organic field effect transistors," *J. Display Technol.*, vol. 1, pp. 289–294, 2005.

[37] V. Jayaraman, Z.-M. Chuang, and L. A. Coldren, "Theory, design, and performance of extended tuning range semiconductor lasers with sampled gratings," *IEEE J. Quantum Electron.*, vol. 29, pp. 1824–1834, 1993.

[38] P. O. Anikeeva, J. E. Halpert, M. G. Bawendi, and V. Bulovic, "Electroluminescence from a mixed red-green-blue colloidal quantum dot monolayer," *Nano Lett.*, vol. 7, p. 2196, 2007.

[39] R. L. Petritz, "Theory of photoconductivity in semiconductor films," *Phys. Rev.*, vol. 104, pp. 1508–1516, 1956.

[40] R. Bube, *Photoconductivity of Solids*. New York: Wiley, 1960.

[41] R. Bube, *Photoelectronic Properties of Semiconductors*. Cambridge, U.K.: Cambridge Univ. Press, 1992.

[42] A. Rose, *Concepts in Photoconductivity and Allied Problems*. Melbourne, FL: Krieger, 1972.

[43] S. Espevik, C. Wu, and R. H. Bube, "Mechanism of photoconductivity in chemically deposited lead sulfide layers," *J. Appl. Phys.*, vol. 42, p. 3513, 1971.

[44] R. Bube and C. T. Ho, "Laser saturation of photoconductivity and determination of imperfection parameters in sensitive photoconductors," *J. Appl. Phys.*, vol. 37, no. 11, pp. 4132–4138, 1966.

[45] E. L. Dereniak and G. D. Boreman, *Infrared Detectors and Systems*. New York: Wiley, 1996.

[46] R. C. Jones, "A method of describing the detectivity of photoconductive cells," *Rev. Sci. Instrum.*, vol. 24, p. 1035, 1953.

[47] G. Yu, K. Pakbaz, and A. J. Heeger, "Semiconducting polymer diodes: Large size, low cost photodetectors with excellent visible-ultraviolet sensitivity," *Appl. Phys. Lett.*, vol. 64, no. 25, pp. 3422–3424, 1994.

[48] G. Yu, J. Wang, J. McElvain, and A. Heeger, "Large-area, full-color image sensors made with semiconducting polymers," *Adv. Mater.*, vol. 10, pp. 1431–1434, 1998.

[49] M. Hamilton, S. Martin, and J. Kanicki, "Thin-film organic polymer phototransistors," *IEEE Trans. Electron Devices*, vol. 51, pp. 877–885, 2004.

[50] P. V. V. Jayaweera, A. G. U. Perera, M. K. I. Senevirathna, P. K. D. D. P. Pitigal, and K. Tennakone, "Dye-sensitized near-infrared room-temperature photovoltaic photodetectors," *Appl. Phys. Lett.*, vol. 85, pp. 5754–5756, 2004.

[51] P. Peumans, V. Bulovic, and S. R. Forrest, "Efficient high-bandwidth organic multilayer photodetectors," *Appl. Phys. Lett.*, vol. 76, pp. 3855–3857, 2000.

[52] N. C. Greenham, X. Peng, and A. P. Alivisatos, "Charge separation and transport in conjugated-polymer/semiconductor-nanocrystal composites studied by photoluminescence quenching and photoconductivity," *Phys. Rev. B*, vol. 54, p. 17 628, 1996.

[53] C. A. Leatherdale, C. R. Kagan, N. Y. Morgan, S. A. Empedocles, M. A. Kastner, and M. G. Bawendi, "Photoconductivity in CdSe quantum dot solids," *Phys. Rev. B*, vol. 62, p. 2669, 2000.

[54] M. V. Jarosz, V. J. Porter, B. R. Fisher, M. A. Kastner, and M. G. Bawendi, "Photoconductivity studies of treated CdSe quantum dot films exhibiting increased exciton ionization efficiency," *Phys. Rev. B*, vol. 70, no. 19, p. 195 327, 2004.

[55] S. A. McDonald, G. Konstantatos, S. Zhang, P. W. Cyr, E. J. D. Klem, L. Levina, and E. H. Sargent, "Solution-processed PbS quantum dot infrared photodetectors and photovoltaics," *Nature Mater.*, vol. 4, pp. 138–142, 2005.

[56] G. Konstantatos, I. Howard, A. Fischer, S. Hoogland, J. Clifford, E. Klem, L. Levina, and E. H. Sargent, "Ultrasensitive solution-cast quantum dot photodetectors," *Nature*, vol. 442, no. 7099, pp. 180–183, 2006.

[57] D. Yu, C. Wang, B. L. Wehrenberg, and P. Guyot-Sionnest, "Variable range hopping conduction in semiconductor nanocrystal solids," *Phys. Rev. Lett.*, vol. 92, p. 216 802, 2004.

[58] D. Talapin and C. B. Murray, "PbSe nanocrystal solids for n- and p-channel thin film field-effect transistors," *Science*, vol. 310, pp. 86–89, 2005.

[59] R. H. Rahada and H. T. Minden, "Photosensitization of PbS Films," *Phys. Rev.*, vol. 102, pp. 1258–1262, 1956.

[60] G. W. Mahlman, "Photoconductivity of lead sulfide films," *Phys. Rev.*, vol. 103, pp. 1619–1630, 1956.

[61] C. Nascu, V. Vomir, I. Pop, V. Ionescu, and R. Grecu, "The study of lead sulphide films, VI. Influence of oxidants on the chemically deposited PbS thin films," *Mater. Sci. Eng. B*, vol. 41, pp. 235–240, 1996.

[62] I. Pop, V. Ionescu, C. Nascu, V. Vomir, R. Grecu, and E. Indrea, "The study of lead sulfide films. The behaviour at low-temperature thermal treatment," *Thin Solid Films*, vol. 283, pp. 119–123, 1996.

[63] A. Carbone and P. Mazzetti, "Grain-boundary effects on photocurrent fluctuations in polycrystalline photoconductors," *Phys. Rev. B*, vol. 57, p. 2454, 1998.

[64] A. Carbone, P. Mazzetti, and F. Rossi, "Low-frequency photocurrent noise in semiconductors: Effect of nonlinear current-voltage characteristics," *Appl. Phys. Lett.*, vol. 78, pp. 2518–2520, 2001.

[65] D. Yu, B. L. Wehrenberg, P. Jha, J. Ma, and P. Guyot-Sionnest, "Electronic transport of n-type CdSe quantum dot films: Effect of film treatment," *J. Appl. Phys.*, vol. 99, p. 104 315, 2006.

[66] G. Konstantatos, J. Clifford, L. Levina, and E. H. Sargent, "Sensitive solution-processed visible-wavelength photodetectors," *Nature Photon.*, vol. 1, pp. 531–534, 2007.

[67] P. P. Suni, "Gain compression photodetector array," U.S. Patent 4 967 249, 1990.

[68] G. Konstantatos and E. H. Sargent, "PbS colloidal quantum dot photoconductive photodetectors: Transport, traps, and gain," *Appl. Phys. Lett.*, vol. 91, no. 17, p. 173 505, 2007.

[69] G. Konstantatos, L. Levina, A. Fischer, and E. H. Sargent, "Engineering the temporal rresponse of photoconductive photodetectors via selective introduction of surface trap states," *Nano Lett.*, vol. 8, pp. 1446–1450, 2008.

[70] J. Clifford, G. Konstantatos, S. Hoogland, L. Levina, and E. Sargent, "Fast, sensitive, spectrally-tunable solution-processed photodiodes," *Nature Nanotechnol.*, to be published.

[71] D. C. Oertel, M. G. Bawendi, A. C. Arango, and V. Bulovic, "Photodetectors based on treated CdSe quantum-dot films," *Appl. Phys. Lett.*, vol. 87, pp. 213 505–213 507, 2005.

[72] J. P. Clifford, K. W. Johnston, L. Levina, and E. H. Sargent, "Schottky barriers to colloidal quantum dot films," *Appl. Phys. Lett.*, vol. 91, no. 25, p. 253 117, 2007.

[73] P. Guyot-Sionnest and C. Wang, "Fast voltammetric and electrochromic response of semiconductor nanocrystal thin films," *J. Phys. Chem. B*, vol. 107, pp. 7355–7359, 2003.

[74] M. Boberl, M. V. Kovalenko, S. Gamerith, E. J. W. List, and W. Heiss, "Inkjet-printed nanocrystal photodetectors operating up to 3 μm wavelengths," *Adv. Mater.*, vol. 19, pp. 3574–3578, 2007.

[75] Y. Jin, J. Wang, B. Sun, J. C. Blakesley, and N. C. Greenham, "Solution-processed ultraviolet photodetectors based on colloidal ZnO nanoparticles," *Nano Lett.*, vol. 8, pp. 1649–1653, 2008.

[76] F. F. Amos, S. A. Morin, J. A. Streifer, R. J. Hamers, and S. Jin, "Photodetector arrays directly assembled onto polymer substrates from aqueous solution," *J. Amer. Chem. Soc.*, vol. 129, no. 46, pp. 14 296–14 302, 2007.

[77] G. Konstantatos, L. Levina, and E. H. Sargent, "Sensitive solution-processed Bi_2S_3 nanocrystalline photodetectors," *Nanoletters*, to be published.

[78] S. Hinds, L. Levina, E. J. D. Klem, G. Konstantatos, V. Sukhovatkin, and E. H. Sargent, "Smooth-morphology ultrasensitive solution-processed photodetectors," *Adv. Mater.*, to be published.

[79] M. Hegg and L. Y. Lin, "Near-field photodetection with high spatial resolution by nanocrystal quantum dots," *Opt. Express*, vol. 15, pp. 17 163–17 170, 2007.

ABOUT THE AUTHORS

Gerasimos Konstantatos received the Diploma from the University of Patras, Patras, Greece, in 2001 and the M.A.Sc. and Ph.D. degrees from University of Toronto, Toronto, ON, Canada, in 2004 and 2008, respectively, all in electrical and computer engineering.

He was a Research Associate with the Electromagnetics Laboratory, Department of Electrical and Computer Engineering, University of Patras, from 2001 to 2002. He joined the Electrical and Computer Engineering Department, University of Toronto, in 2002. He is currently a Group Leader and Assistant Professor with the Institute of Photonic Sciences, Castelldefels, Barcelona, Spain.

Edward H. (Ted) Sargent received the B.Sc.Eng. degree in engineering physics from Queen's University, Kingston, ON, Canada, in 1995, and the Ph.D. degree in electrical and computer engineering (Photonics) from the University of Toronto, Toronto, ON, Canada, in 1998.

He is a Professor and holder of the Canada Research Chair in Nanotechnology at the University of Toronto. In 2004–2006, he was also a Visiting Professor of Nanotechnology at the Massachusetts Institute of Technology, Cambridge.

Dr. Sargent was named "one of the world's top young innovators" by MIT's *Technology Review* in 2003. In 2002, the Canadian Institute for Advanced Research named him one of Canada's top 20 researchers under age 40. In 2002, he received the Outstanding Engineer Award from IEEE Canada. He received the 1999 NSERC Silver Medal.